Precipitation behavior and hardness response of Alloy 625 weld overlay under different aging conditions

Article *in* Welding in the World, Le Soudage Dans Le Monde · March 2019

DOI: 10.1007/s40194-019-00724-1

CITATIONS
0

READS
103

4 authors, including:

Tao Dai
The Ohio State University
11 PUBLICATIONS **26** CITATIONS
SEE PROFILE

Rebecca Ann Wheeling
The Ohio State University
4 PUBLICATIONS **3** CITATIONS
SEE PROFILE

Welding in the World
https://doi.org/10.1007/s40194-019-00724-1

RESEARCH PAPER

Precipitation behavior and hardness response of Alloy 625 weld overlay under different aging conditions

T. Dai[1] · R. A. Wheeling[1] · K. Hartman-Vaeth[1] · J. C. Lippold[1]

Received: 7 October 2018 / Accepted: 27 February 2019

Abstract
The hardness response of Alloy 625 weld overlay on low alloy steel was evaluated under a range of aging conditions to determine how the properties of the overlay change during postweld heat treatment (PWHT). It was presumed that the hardening compared to the as-welded condition occurs due to the precipitation of gamma double-prime (γ''). To confirm this assumption, an investigation was conducted on weld overlay samples under different aging conditions, using Vickers hardness testing, SEM microstructure characterization, SEM/EDAX analysis, and nanoindentation. The Alloy 625 weld overlay hardness values initially increased but eventually decreased with increasing aging temperature. γ'' precipitation was found in the interdendritic regions of the weld overlay samples. In the overaged condition, dissolution and coarsening of γ'' precipitates occurred. Delta (δ) phase also formed in the interdendritic regions, generally at higher temperatures than for γ'' precipitation. Nanoindentation revealed that the precipitation of γ'' is responsible for the hardening in the interdendritic regions of Alloy 625 weld overlay. The time-temperature-precipitation curves of interdendritic regions are altered from that of wrought Alloy 625 due to higher Nb, Ti, and Mo contents and lower dislocation density. The peak temperatures achieved in service for heating coke drum may result in interdendritic γ'' precipitation which can cause significant hardening of the overlay and promote cracking.

Keywords Alloy 625 · Weld overlay · Aging behavior · Hardness · Microstructure characterization · Interdendritic · Gamma double-prime precipitation

1 Introduction

Nickel-chromium-molybdenum Alloy 625 was patented in 1964 and since then it has been used in applications that require excellent resistance to corrosion, oxidation, and elevated temperature creep. Its tensile strength, ductility, and impact toughness are also good at cryogenic temperatures. Alloy 625 weld metal (ERNiCrMo-3 type) has demonstrated good weldability and resistance to hot cracking for shielded metal arc, gas metal arc, gas tungsten arc, and submerged arc welding processes [1].

Alloy 625 filler metal is widely used to clad steel components for corrosion protection at ambient or elevated service temperatures. In the oil and gas industry, the inner pipeline surfaces or connectors are often clad with Alloy 625. The clad weldment may be tempered (postweld heat treatment or PWHT) in the range of 620–670 °C to reduce the steel HAZ hardness and relieve residual stresses. The hardness of the Alloy 625 weld overlay increases after PWHT [2–5] and may possibly continue to harden in service, depending on the service temperature. Recently, the Alloy 625 weld overlay on a coke drum was found to contain cracks. It was reported that the coke drum experienced cyclic heating up to 480 °C (895 °F) and the cracks may result from the reduced ductility associated with the hardening of the weld overlay [6] coupled with thermomechanical fatigue conditions from thermal cycling. The authors hypothesized that precipitation of gamma double-prime phase (γ'') is responsible for the hardening mechanism in the Alloy 625 weld overlay and hence, a system more susceptible to thermomechanical fatigue. If a ductility drop accompanied a strength increase, material compliance responsible for relieving residual stress accumulated may be reduced. The stoichiometry of the γ'' phase is $Ni_3(Al,Ti,Nb)$ in an ordered body-centered tetragonal DO_{22} structure [7–9].

Recommended for publication by Commission IX - Behaviour of Metals Subjected to Welding

✉ T. Dai
dai.234@osu.edu

[1] Welding Engineering Program, The Ohio State University, Columbus, OH, USA

Published online: 14 March 2019

There are few studies on the precipitation behavior of Alloy 625 weld overlays, other than the work of Petrzak et al. [10], but the precipitation behavior in other (base metal) forms of Alloy 625 has been reported. Shaikh et al. [11] studied Alloy 625 sheet samples after solution heat treatment, quenching, and aging. They reported the precipitation of γ″ at aging temperatures of 700 and 760 °C, and nucleation of γ″ at temperatures down to 625 °C. Suave et al. [12] reported the precipitation of γ″ in the temperature range 550–750 °C and the precipitation of δ-phase in the temperature range 650–900 °C in the as-rolled and solution treated sheet material. Malej et al. [13] studied the aging of Alloy 625 rolled plate at 650 °C and the precipitation of γ″ and δ-phase were first observed after 25 and 504 h, respectively. In Mathew's work [14], γ″ phase was found at 700 °C with a disc-shaped morphology after 500 h. Acicular δ-phase was observed in a re-solution annealed Alloy 625 in the temperature range 650–825 °C and the morphology changed significantly with the increase of temperature. $M_{23}C_6$ carbides were also found at the grain boundaries [14]. Floreen [9] reported that the γ″ precipitation range is 593–760 °C and γ″ denuded zones were found around the grain boundaries and Nb-rich particles. Ti and Al are necessary for γ″ precipitation [8] as decreasing Ti + Al content has been shown to decrease precipitation hardening by γ″ [9] [15]. No precipitation of γ″ was observed in Alloy 625 in which Ti and Al were absent, although formation of δ phase is still possible. γ″ precipitation in the range of 600–800 °C is reported to promote a ductility loss in the Alloy 625 [8].

In summary, most of the studies of γ″ precipitation in Alloy 625 have been conducted with homogenized base metals or after prescribed thermomechanical processing. The only study on precipitation of γ″ in Alloy 625 weld metal was from Petrzak et al. [10], but the data in this study was very limited. In order to understand the precipitation and hardening effects in Alloy 625 weld overlay, 10 different aging conditions were investigated. SEM and EDX were used to characterize the precipitation. Micro- and nanohardness techniques were used to understand the hardening reaction of the aged Alloy 625 weld overlay.

2 Experimental procedures

To demonstrate that hardening of the Alloy 625 overlay can occur during PWHT and/or during service exposure, a boat sample from service field and a three-layer Alloy 625 clad sample were provided by AZZ/WSI®. The compositions of base metal and weld metal are in Table 1. This sample was produced using the temper bead welding procedure with the welding parameters in Table 2 and Table 3.

Ten samples were cut from the as-welded Alloy 625 overlay and they were postweld heat-treated at 10 different aging conditions as listed in Table 1. Samples for metallurgical analysis were ground and polished and then etched electrolytically using a 10% chromic acid solution at 5 V for 10–15 s to reveal the microstructure of the weld sample. This technique is described as a "matrix" etch, whereby the austenitic (fcc) matrix is etched away leaving precipitates exposed on the etched surface. These samples were examined in the scanning electron microscope (SEM). SEM/EDAX mapping was used to measure chemical composition distribution. EDAX point analysis was used to measure the chemical composition in the dendrite core and interdendritic regions. Several points were selected in both regions to obtain the average compositions.

The furnace-aged samples (Table 4) and an overlay sample removed from a coke drum were polished through a 6-μm-type diamond paste for microhardness examination. A microhardness map was generated using a load of 300 gf ($HV_{0.3}$) and a step size of 0.3 mm between indents. Based on the Vickers hardness response, nanoindentation was conducted on a sample aged at 1400 °F/10 h to determine the hardness distribution in the dendritic microstructure. This sample was polished through 1-μm-type diamond paste and was polished manually using a 0.5-μm-type colloidal solution. An MTS NanoIndenter XP system was used to create a nanohardness map on the sample. The XP load control mode was selected and the maximum load of each nanoindentation is 2gf, with a step size of 6 μm.

3 Results

3.1 Hardening of Alloy 625 weld overlay

The location of the hardness map relative to the 3-layer Alloy 625 weld overlay from a sample removed from the coke drum is shown in Fig. 1a. The arrows show the location of the fusion boundary between the first clad layer and the steel. A compilation of the hardness data including all the points in this hardness map is shown in Fig. 1b. The steel is ASTM A387, grade 11. This is a nominal 1.25Cr-0.5Mo-0.1C pressure

Table 1 Chemical compositions of base metal and weld metal (filler wire)

	C	Mn	Fe	P	S	Si	Cu	Ni	Al	Ti	Cr	Ta	Mo	Other elements total
BM carbon steel	0.28	0.85–1.20	Bal.	< 0.25	< 0.25	0.15–0.40	–	–	–	–	–	–	–	–
WM ERNiCrMo-3	0.10	0.50	5.0	0.02	0.015	0.50	0.50	58.0	0.40	0.40	20.0–23.0	3.15–4.15	8.0–10.0	0.50

Table 2 Welding type and parameters

Welding type	Preheat temp.	Interpass temp.	PWHT	Shielding gas	Flow rate	Filler size	Current
GMAW	93.3 °C (200 °F)	287.8 °C (550 °F)	233 °C (450 °F) for 4 h	100% argon	14–26 L/min (30–55 CFH)	1.143mm (0.045 in.)	DCEP

vessel steel that would be expected to form mostly untempered bainite and martensite in the HAZ. Peak HAZ hardness on the order of 350 $HV_{0.3}$ would be consistent for this steel, considering that some tempering may occur during application of the 2nd and 3rd cladding layers and possibly during service exposure.

As-deposited Alloy 625 cladding normally exhibits hardness in the range from 250 to 280 VHN. Thus, the cladding in this service-exposed sample is much higher than when it was put into service, indicating that hardening has occurred during service. The difference in hardness between the 1st layer and the 2nd/3rd layers is due to the dilution of the Alloy 625 by the steel in the 1st layer. The dilution effect is also apparent by the difference in etching characteristics of the 1st layer, as shown in Fig. 1a.

The increase in hardness of the service-exposed overlay presumably occurs due to age hardening of the overlay in service. Since Alloy 625 contains on the order of 3.5 wt% Nb, the formation of γ'' can occur if heated into the appropriate temperature range. The formation of substantial γ'' would result in an increase in overlay hardness. The microstructure of the 3rd layer of the overlay after matrix etching is shown in Fig. 2. In the low-magnification SEM micrograph, the partitioning of Nb can clearly be seen as the lighter areas at the interdendritic boundaries. At higher magnification, actual precipitates can be observed and these are presumably Nb-rich γ''.

The microhardness data for the aged Alloy 625 samples prepared in the laboratory and heat-treated per the conditions shown in Table 4 are shown in Fig. 3. The hardness in the as-welded condition is the lowest. The highest hardness occurs after aging at 1300 °F/100 h where the average hardness reached 326 $HV_{0.3}$, which is lower than that of the sample from the field. This may be the result of a much longer aging time in service which results in further hardening of the Alloy 625 weld overlay or clad actual composition richer in Nb, Al, Ti (still within the Alloy 625 nominal composition range). Aging at higher temperatures in the range 760–871 °C (1400–1600 °F) reduced the hardness of the Alloy 625 weld overlay below the peak value, probably due to overaging.

3.2 Precipitation phenomenon

Microstructure characterization was used to explain the hardening effect of the aged samples. After aging at 1200 °F for 10 h, no obvious precipitation was observed except for the blocky particles (Fig. 4a), even in the interdendritic regions (Fig. 4b). Since the hardness of sample 1200 °F/10 h is higher than the as-welded sample, initial nucleation of precipitates may have promoted the slight hardening, but precipitates may be too small to be observed using metallographic techniques. The blocky particles in Fig. 4a formed during the solidification and are presumably primary MC carbides with Nb, Ti, and Mo. These are very stable carbides and do not dissolve at any of the aging temperatures used in this study. Thus, the blocky particles are observed in all the aged samples.

It is easier to distinguish the small precipitates after the 1200 °F/100 h heat treatment, as shown in Figs. 4 c and d. These precipitates are in the interdendritic regions. After the 1300 °F/10 h heat treatment, a sparse distribution of precipitates was also observed in the interdendritic regions as shown in Fig. 4f. A precipitation denuded zone can be seen around the blocky particle in Fig. 4f. Because the strong carbide formers, Nb and Ti, combined with C to form the blocky MC carbides, the surrounding matrix is depleted and γ'' precipitates do not form in the adjacent area. Aging at 1300 °F for 100 h, the precipitates are clearly apparent in the interdendritic regions with precipitate-free zones at the dendrite cores (Fig. 4g, h). They are presumed to be mainly γ'' phase according to the typical morphology and the aging temperature range.

After aging at 1400 °F for 1 h, the interdendritic regions could be clearly distinguished and a needle-shaped phase was observed (Fig. 5b), presumably δ phase. Although γ'' phase may be present, it is hard to distinguish. After aging at 1400 °F

Table 3 Additional welding parameters

Welding parameters	Current	Voltage	Travel steep	Wire feed speed
Layer 1	170–175 A	23–24 V	762 mm/min (30 in./min)	5080–6350 mm/min (200–250 in./min)
Layer 2	190–195 A	24–25 V	635 mm/min (25 in./min)	6096–7112 mm/min (240–280 in./min)
Layer 3	210–220 A	26–28 V	635 mm/min (25 in./min)	7112–9652 mm/min (280–380 in./min)
Reminder layer if any	210–220 A	26–28 V	635 mm/min (25 in./min)	7112–9652 mm/min (280–380 in./min)

Table 4 Aging conditions of Alloy 625 weld overlay samples (water quench after aging)

	1	2	3	4	5	6	7	8	9	10
Holding temperature	1200 °F (649 °C)	1200 °F (649 °C)	1300 °F (704 °C)	1300 °F (704 °C)	1400 °F (760 °C)	1400 °F (760 °C)	1500 °F (816 °C)	1500 °F (816 °C)	1600 °F (871 °C)	1600 °F (871 °C)
Holding time	10 h	100 h	10 h	100 h	1 h	10 h	1 h	10 h	1 h	10 h

for 10 h, γ'' precipitates can be observed with an elliptical shape, up to 100 nm in length. There are also some plate-shaped precipitates that are probably δ phase. Heavy precipitation can be seen in the interdendritic regions (Fig. 5c–f) and the dendrite core regions contain few precipitates as shown in Fig. 5f. The area with dense precipitation (Fig. 5c) appears to be reduced compared to the 1400 °F/1 h condition (Fig. 5a) probably due to the higher local density of precipitates in the interdendritic regions that form during extended aging at 1400 °F.

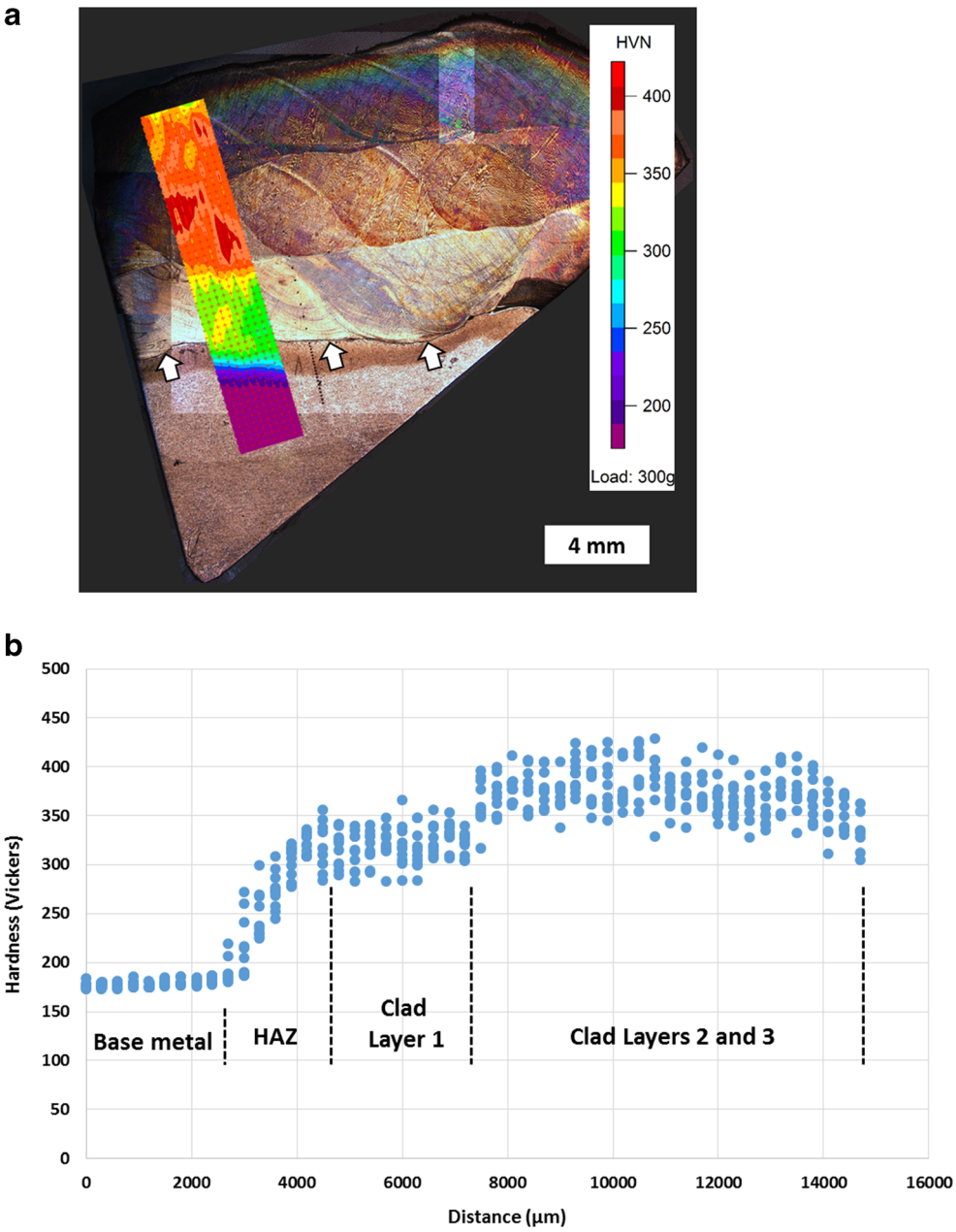

Fig. 1 Hardness map across the clad interface of a boat sample removed from the coke drum. **a** Location of hardness map. **b** Compilation of hardness data within the hardness map

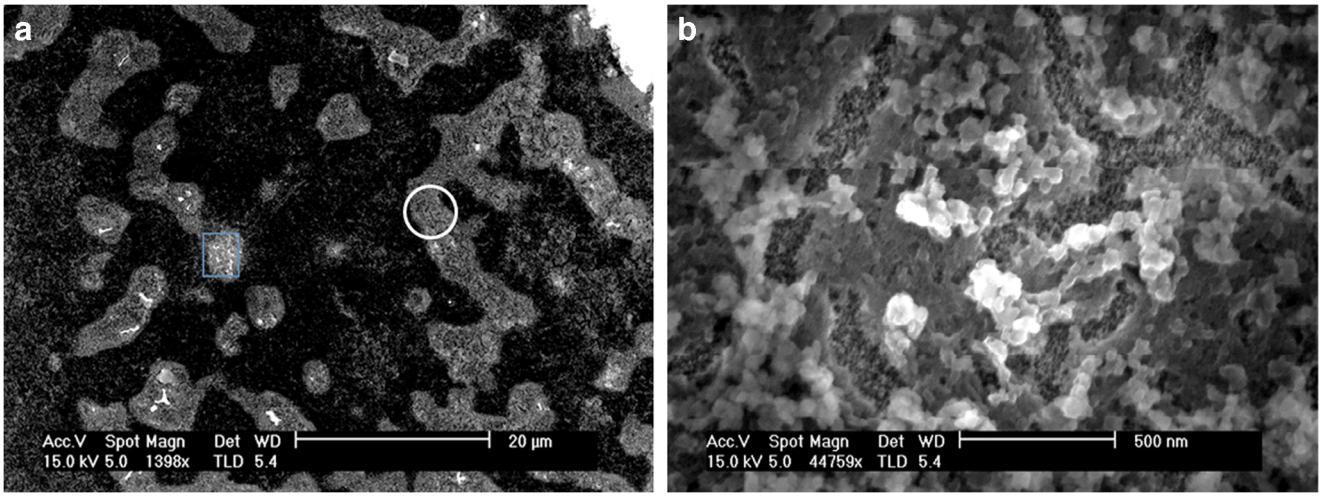

Fig. 2 Service-exposed Alloy 625 overlay after "matrix" etch. **a** Low magnification SEM micrograph from 3rd layer of overlay, **b** high magnification (× 45,000) showing precipitates. The lighter areas in **a** correspond to regions of high Nb content due to solidification segregation

The interdendritic regions after 1500 °F/1 h contain both elliptical-shaped γ″ precipitates and needle-like δ phase as shown in Figs. 6 a and b. The sample aged at 1500 °F/1 h exhibits a less dense interdendritic precipitation distribution than the sample aged at 1400 °F/1 h. Comparing Fig. 6a and Fig. 6c, the clusters of δ phase present after aging 1500 °F/10 h appear to have almost completely replaced the γ″ phase, and the few remaining γ″ precipitates coarsened to 100–300 nm in length (Fig. 6d). The density of γ″ precipitates decreased greatly compared with Fig. 6b. Aging at 1600 °F results in the formation of even more plate-shaped δ phase. At 1600 °F/1 h in Figs. 6e and f, both the plate-like δ phase and γ″ co-exist in the interdendritic regions with the area of precipitation decreasing relative to the 1400 and 1500 °F heat treatments. Comparing to 1 and 10 h aging conditions in Figs. 6 c and g, it can be seen that the clusters of δ phase are more concentrated with thicker δ phase as aging time increases. This is probably due to the fact that the δ phase (Ni_3Nb) consumes more Nb than the γ″ precipitate.

3.3 EDAX mapping

As a representative example, the result of SEM/EDAX mapping of the 1400 °F/10 h sample is shown in Fig. 7. Four phase fields were present in the EDAX map: blue, red, yellow, and green and the composition of each phase field is shown in Table 5. The dendrite core regions mainly consist of blue and red phase fields. The content of Nb, Mo, and Ti in this region is relatively low due to segregation during the solidification process (Table 5). The interdendritic regions mainly consist of yellow phase and also small portion red phase. Table 5 shows that the interdendritic regions have higher content of Nb, Mo, and Ti, which are responsible for the precipitation during aging. The green phase field is only 1% of the EDX map and corresponds to blocky particles (Fig. 7a, b), which contain high content of Mo (13.79 wt%) and extremely high content of Nb (18.32 wt%) and Ti (2.08 wt%). These are most likely the MC carbides that form via a eutectic reaction at the end of solidification. The size of any γ″ precipitates

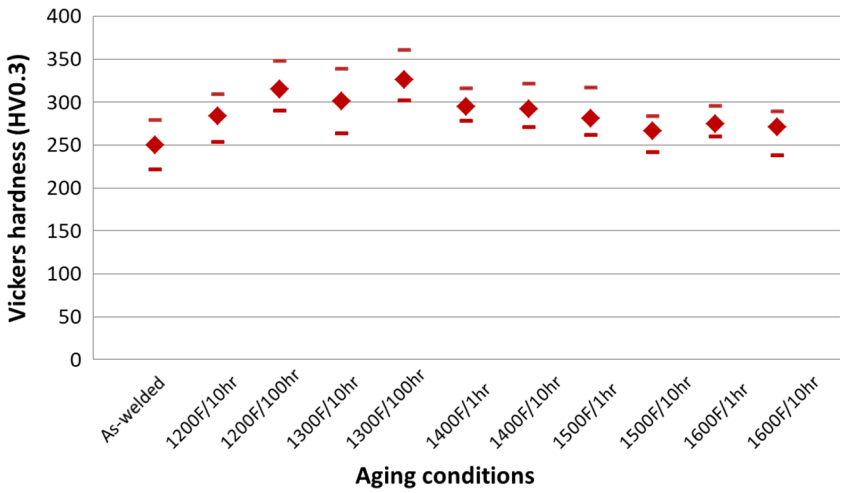

Fig. 3 Microhardness of Alloy 625 weld overlay samples in different aging conditions. The average hardness values are shown with error bars

present in any of the samples is less than the approximate 1-μm spatial resolution of the EDAX detector, hence not distinguishable on the map.

3.4 Nanoindentation

The chemical composition and phase distributions in the microstructure of Alloy 625 weld overlay samples are inhomogeneous. Using Vickers hardness testing with an applied load of 300 g and the step size of 300 μm, only a general averaged microhardness or VHN can be measured and much of the detailed information of hardness distribution associated with γ″ and δ phase formation cannot be captured. Nanoindentation is a better tool to measure the hardness distribution on the scale of the solidification substructure. As an example, Alloy 625 weld sample 1400 °F/10 h shows a distinct difference of phase distribution between the dendrite core and interdendritic regions (Fig. 5c and Fig. 7a). Figures 8a and 9b, respectively, show the indents matrix and corresponding nanohardness map. After electrolytically etching with chromic acid, the dendrite core and interdendritic regions are revealed allowing the location of the indentations to be seen (Fig. 8c). Overlapping the nanohardness map on the microstructure, it is evident that the low hardness regions match the dendrite core regions and the high hardness regions match the interdendritic regions (Fig. 8d).

A higher magnification in the yellow framed region of Fig. 8c is shown in Fig. 9. Clearly, the indentations in the dendrite core regions show lower hardness than those in the interdendritic regions with a high density of γ″ precipitates. Also, when the nanoindentation encounters the blocky MC carbides, the hardness is especially high, up to 7.476 GPa, which is the highest hardness spot in Fig. 9.

4 Discussion

4.1 Precipitation behavior and hardness

In the microstructure of Alloy 625 weld overlay samples in the as-welded condition or aged condition, large, blocky particles are observed (Figs. 4a, f; 5d, 6h). EDAX analysis shows that these particles contain high levels of Nb, Mo, and Ti and the presence of C and N. Based on previous work, these particles are MC or M(C,N) that form either during or in the final stages of solidification. The general stoichiometry of these particles are (Nb, Mo, Ti)(C, N) and there are specific phases NbC, TiN, (Nb,Ti)C, Ti(CN) [16], or a mixture of these that may form in Alloy 625 weld metal. As reported by Silva et al. [16], the particles may have TiN as the core and NbC as the shell in an as-solidified Alloy 625 weld overlay. TiN and NbC have the melting point 2927 and 1325 °C respectively and both are stable phases. Thus, the TiN forms above the liquidus temperature and the NbC at the end of solidification in the interdendritic regions. The solidification range of Alloy 625 is reported to be 1290–1350 °C [17]. The presence of these particles may influence the hardness of the weld metal, but they are not the cause of increased hardening during aging since they are present in the as-welded microstructure.

Based on morphology, the interdendritic precipitates in samples aged at 1200 °F/100 h, 1300 °F/10 h, and sample 1300 °F/100 h are most likely the γ″ phase (Fig. 4). Floreen et al. [9] also reported that γ″ precipitation occurs in temperature range 1100–1400 °F in Alloy 625. When aging at 1300 °F for 10 h, the weld metal microstructure exhibits only limited γ″ precipitation. However, after continuous aging at 1300 °F for 100 h, a high density of γ″ precipitates are formed in the interdendritic regions and the hardness reached a maximum (Fig. 3). Sample 1300 °F/100 h has higher hardness than sample 1200 °F/100 h, indicating that the 1300 °F/100 h represents a peak aging condition.

For overlay samples aged at 1400 °F, the hardness decreased due to an apparent overaging condition. In effect, the size of γ″ precipitates increased over some critical value, beyond which the hardening effect started to decrease. In addition, the interdendritic regions of the overlay aged at 1400 °F/10 h contain a mixture of γ″ phase and δ phase. δ phase does not contribute significantly to any hardness increase due to its morphology. Also, aging at 1400 °F resulted in a more localized precipitation in the interdendritic regions resulting in a higher area/volume fraction microstructure that is precipitate-free. As a result, the overall hardness of the sample decreased. Aging at 1500 and 1600 °F results in continued hardness decrease due to additional δ phase transformation and a smaller fraction of coarsened γ″ precipitates.

γ″ is a metastable Ni_3Nb (DO_{22}) phase and δ phase is the stable Ni_3Nb (DO_a) phase [8]. In this work, the δ phase appeared to form when aged at 1400 °F, but only to a limited extent. The δ phase became dominant over γ″ phase at 1500 and 1600 °F. With the increase in the amount of δ phase formation at 1500 and 1600 °F, more localized precipitation in the interdendritic regions left larger precipitate-free areas. As a result, the overall hardness of the overlay decreased. The clusters of δ phase have a lower hardening effect relative to γ″, since they are large, on the order of several microns, and in aging conditions 1500 and 1600 °F/10 h.

Fig. 4 Microstructure of Alloy 625 weld overlay samples in different aging conditions: **a** 1200 °F/10 h, **b** 1200 °F/10 h in interdendritic region, **c** 1200 °F/100 h, **d** higher magnification of the yellow framed area in **c**, **e** 1300 °F/10 h, **f** higher magnification of the yellow framed area in **e**, **g** 1300 °F/100 h, and **h** higher magnification of the yellow framed area in **g**

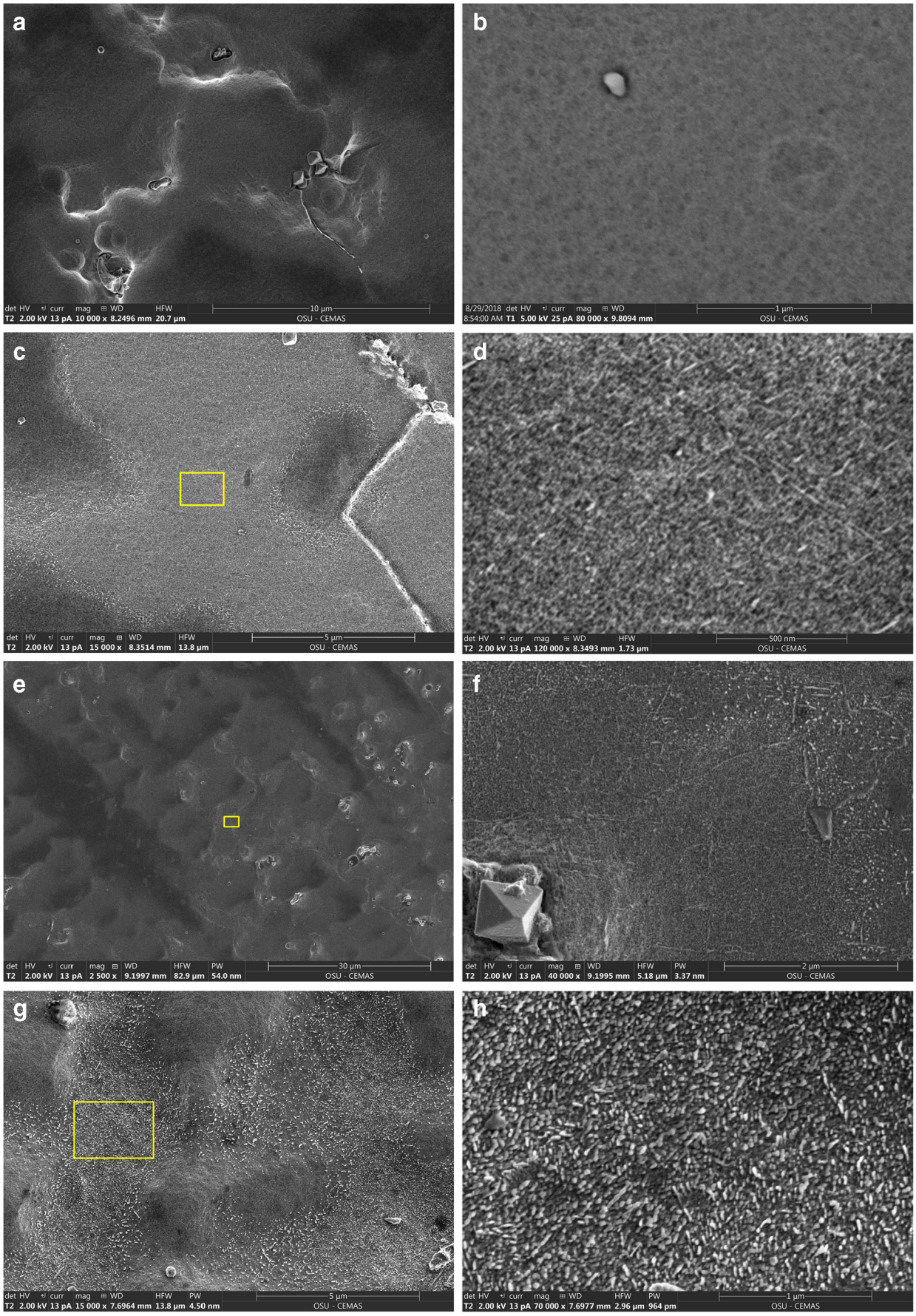
a
det HV curr mag WD HFW
T2 2.00 kV 13 pA 10 000 x 8.2496 mm 20.7 µm
10 µm
OSU - CEMAS
b
8/29/2018 det HV curr mag WD
8:54:00 AM T1 5.00 kV 25 pA 80 000 x 9.8094 mm
1 µm
OSU - CEMAS
c
det HV curr mag WD HFW
T2 2.00 kV 13 pA 15 000 x 8.3514 mm 13.8 µm
5 µm
OSU - CEMAS
d
det HV curr mag WD HFW
T2 2.00 kV 13 pA 120 000 x 8.3493 mm 1.73 µm
500 nm
OSU - CEMAS
e
det HV curr mag WD HFW PW
T2 2.00 kV 13 pA 2 500 x 9.1997 mm 82.9 µm 54.0 nm
30 µm
OSU - CEMAS
f
det HV curr mag WD HFW PW
T2 2.00 kV 13 pA 40 000 x 9.1995 mm 5.18 µm 3.37 nm
2 µm
OSU - CEMAS
g
det HV curr mag WD HFW PW
T2 2.00 kV 13 pA 15 000 x 7.6964 mm 13.8 µm 4.50 nm
5 µm
OSU - CEMAS
h
det HV curr mag WD HFW PW
T2 2.00 kV 13 pA 70 000 x 7.6977 mm 2.96 µm 964 pm
1 µm
OSU - CEMAS

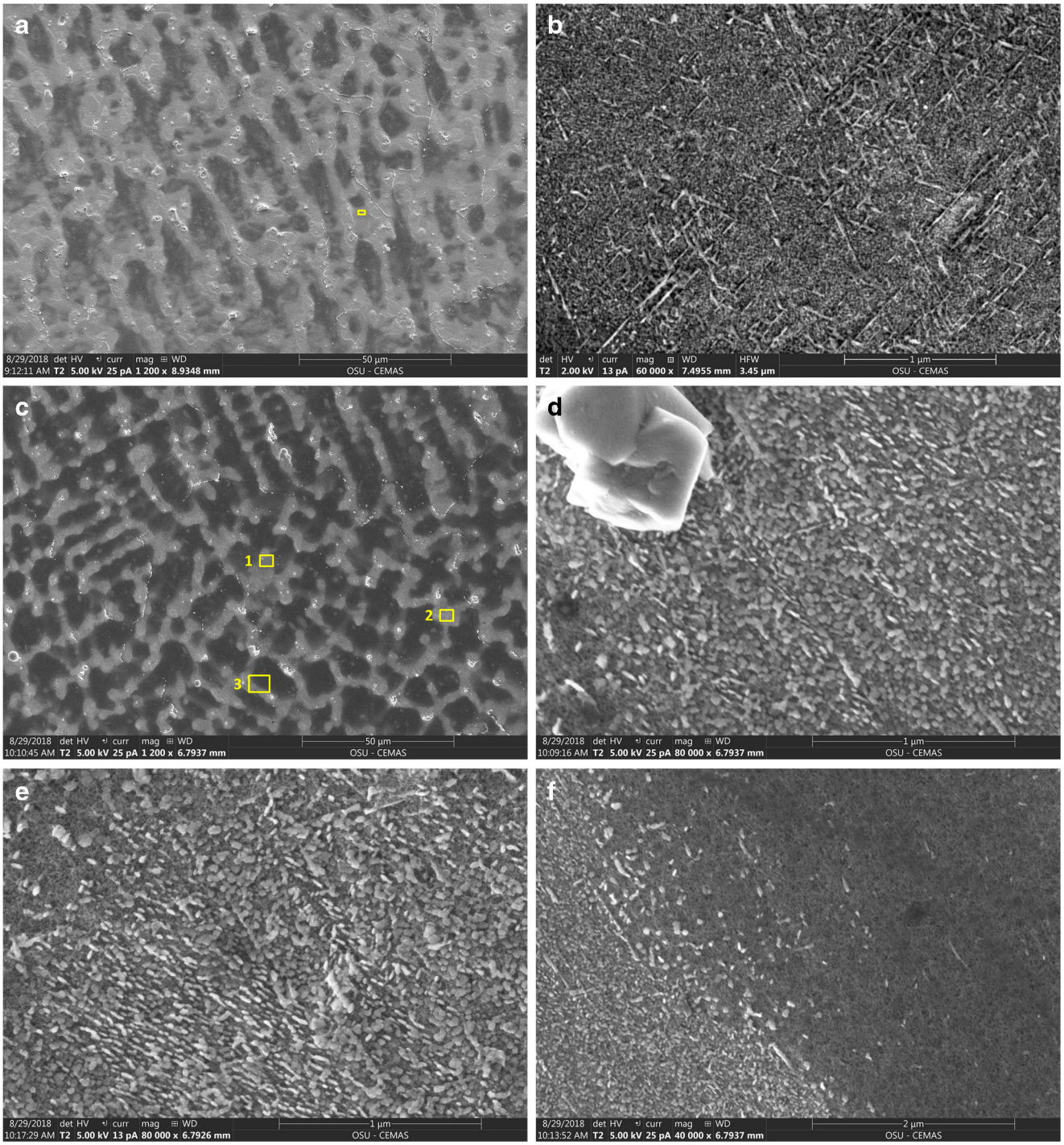

Fig. 5 Microstructure of Alloy 625 weld overlay samples in different aging conditions: **a** 1400 °F/1 h, **b** higher magnification of the yellow framed area in Fig. 4a, **c** 1400 °F/10 h, **d** higher magnification of the yellow framed area 1 in Fig. 4c, **e** higher magnification of the yellow framed area 2, **f** higher magnification of the yellow framed area 3

Fig. 6 Microstructure of Alloy 625 weld overlay samples in different aging conditions, **a** 1500 °F/1 h, **b** higher magnification in the yellow framed area in **a**, **c** 1500 °F/10 h, **d** higher magnification in the yellow framed area in **c**, **e** 1600 °F/1 h, **f** higher magnification in the yellow framed area in **e**, **g** 1600 °F/10 h, **h** higher magnification in the yellow framed area in **g**

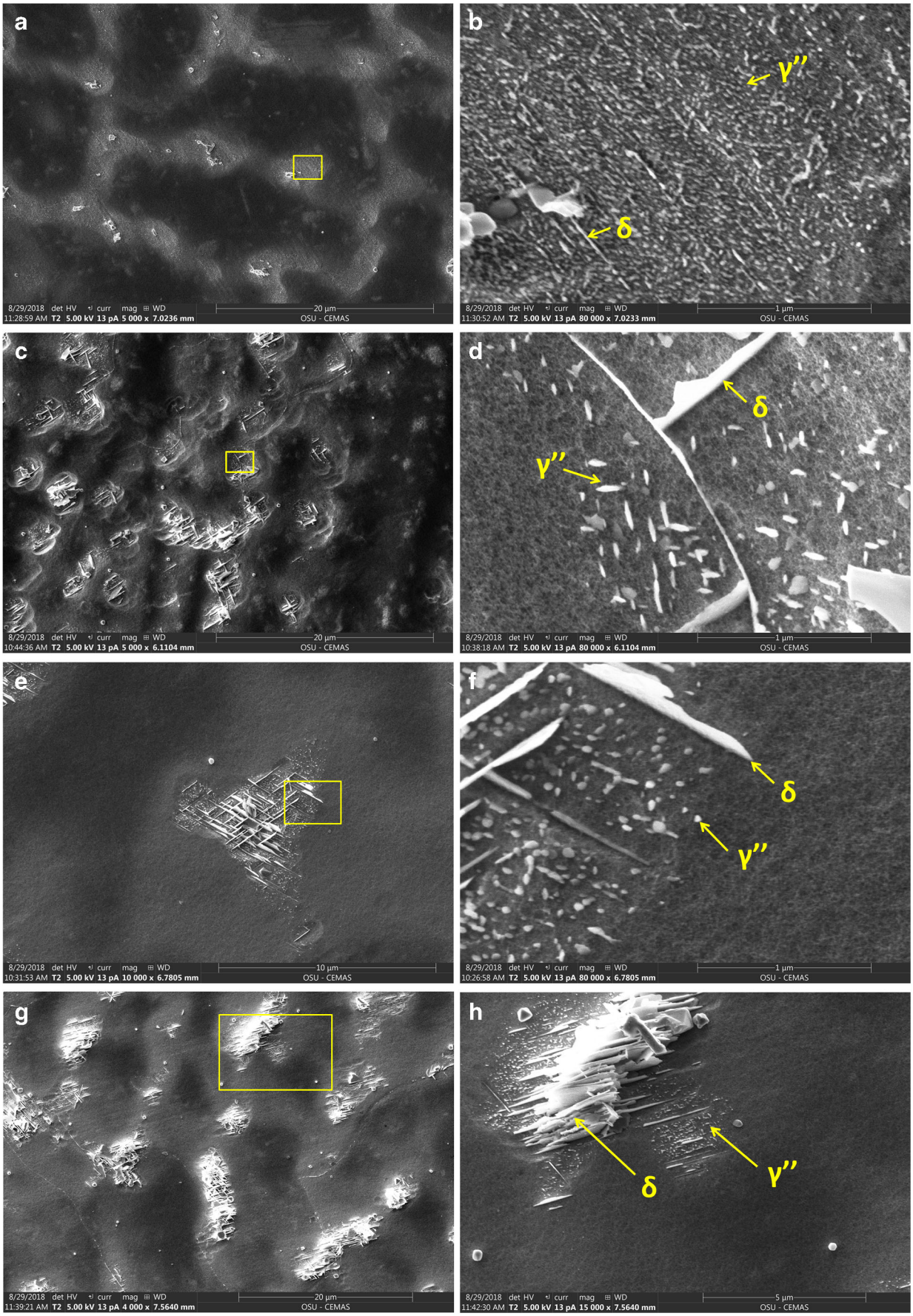
a
8/29/2018 det HV curr mag WD
11:28:59 AM T2 5.00 kV 13 pA 5 000 x 7.0236 mm
20 µm
OSU - CEMAS
b
γ''
δ
8/29/2018 det HV curr mag WD
11:30:52 AM T2 5.00 kV 13 pA 80 000 x 7.0233 mm
1 µm
OSU - CEMAS
c
8/29/2018 det HV curr mag WD
10:44:36 AM T2 5.00 kV 13 pA 5 000 x 6.1104 mm
20 µm
OSU - CEMAS
d
δ
γ''
8/29/2018 det HV curr mag WD
10:38:18 AM T2 5.00 kV 13 pA 80 000 x 6.1104 mm
1 µm
OSU - CEMAS
e
8/29/2018 det HV curr mag WD
10:31:53 AM T2 5.00 kV 13 pA 10 000 x 6.7805 mm
10 µm
OSU - CEMAS
f
δ
γ''
8/29/2018 det HV curr mag WD
10:26:58 AM T2 5.00 kV 13 pA 80 000 x 6.7805 mm
1 µm
OSU - CEMAS
g
8/29/2018 det HV curr mag WD
11:39:21 AM T2 5.00 kV 13 pA 4 000 x 7.5640 mm
20 µm
OSU - CEMAS
h
δ
γ''
8/29/2018 det HV curr mag WD
11:42:30 AM T2 5.00 kV 13 pA 15 000 x 7.5640 mm
5 µm
OSU - CEMAS

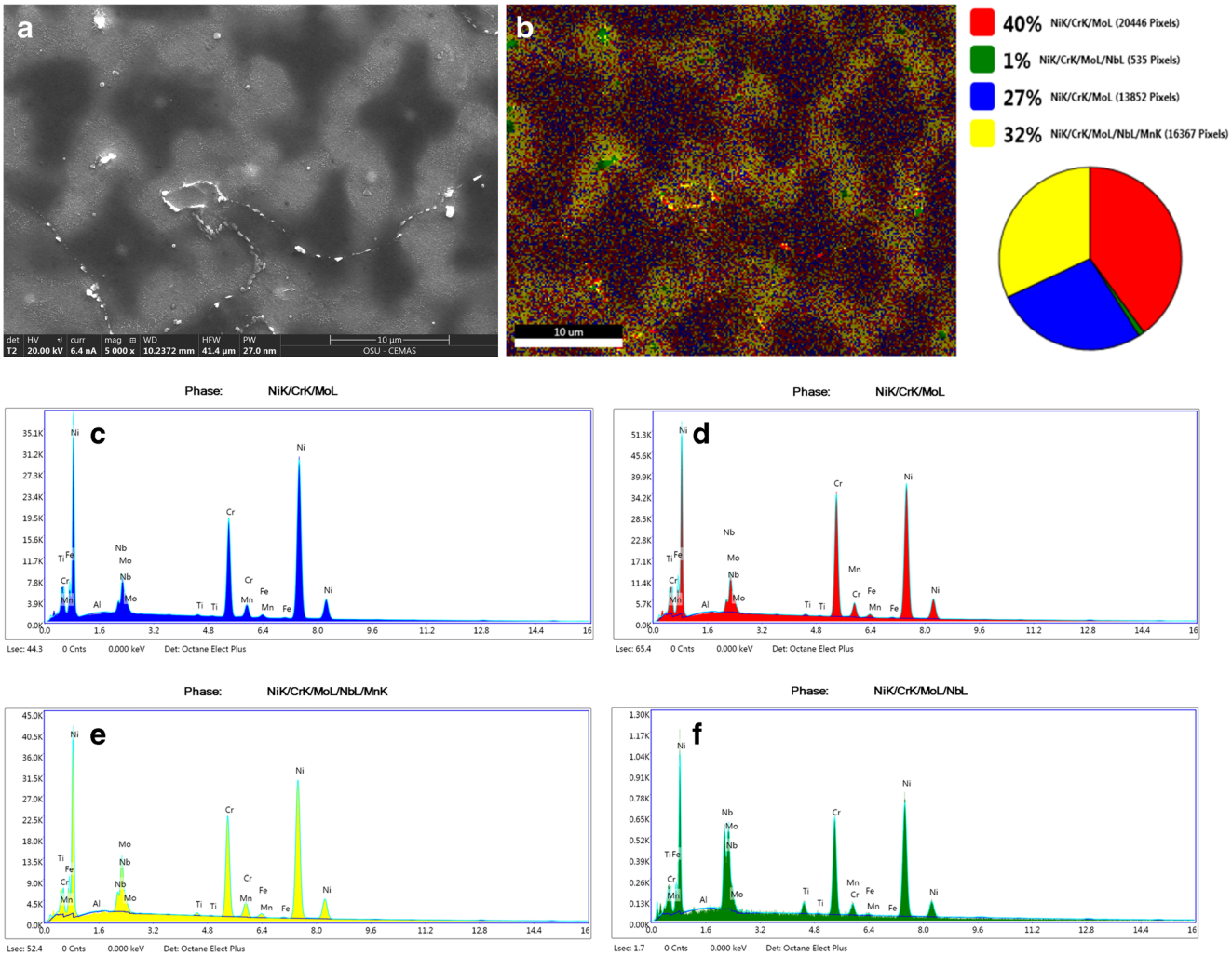

Fig. 7 The sample with aging condition 1400 °F/10r as a representative **a** microstructure for EDAX mapping, **b** EDAX map from **a**, **c**–**f** the spectrums of four different phase fields

4.2 Hardening of the Alloy 625 coke drum weld overlay

According to available information, the nominal peak temperature during coke drum cycling is from 475 to 500 °C (885 to 930 °F). Based on the time-temperature-precipitation (TTP) diagram for Alloy 625 shown in Fig. 10a [1] [9], this range should be well below the γ'' phase formation range. As shown in this figure, temperatures above 1000 °F would be required to form γ'' phase with the "nose" of the range at 670 °C (1240 °F). However, it should be noted that TTP diagram in Fig. 10 was developed for Alloy 625 base metal which was fully homogenized prior to aging.

Table 5 Chemical composition of four phase fields shown in Fig. 7

Elements	Blue phase field (wt%)	Red phase field (wt%)	Yellow phase field (wt%)	Green phase field (wt%)
Nb	2.97	3.27	5.04	18.32
Mo	8.72	9.35	12.49	13.79
Ti	0.30	0.36	0.53	2.08
Cr	22.37	29.04	23.52	21.80
Mn	0.30	0.17	0.52	0.51
Fe	0.93	1.03	1.11	0.56
Ni	64.40	56.78	56.78	42.94

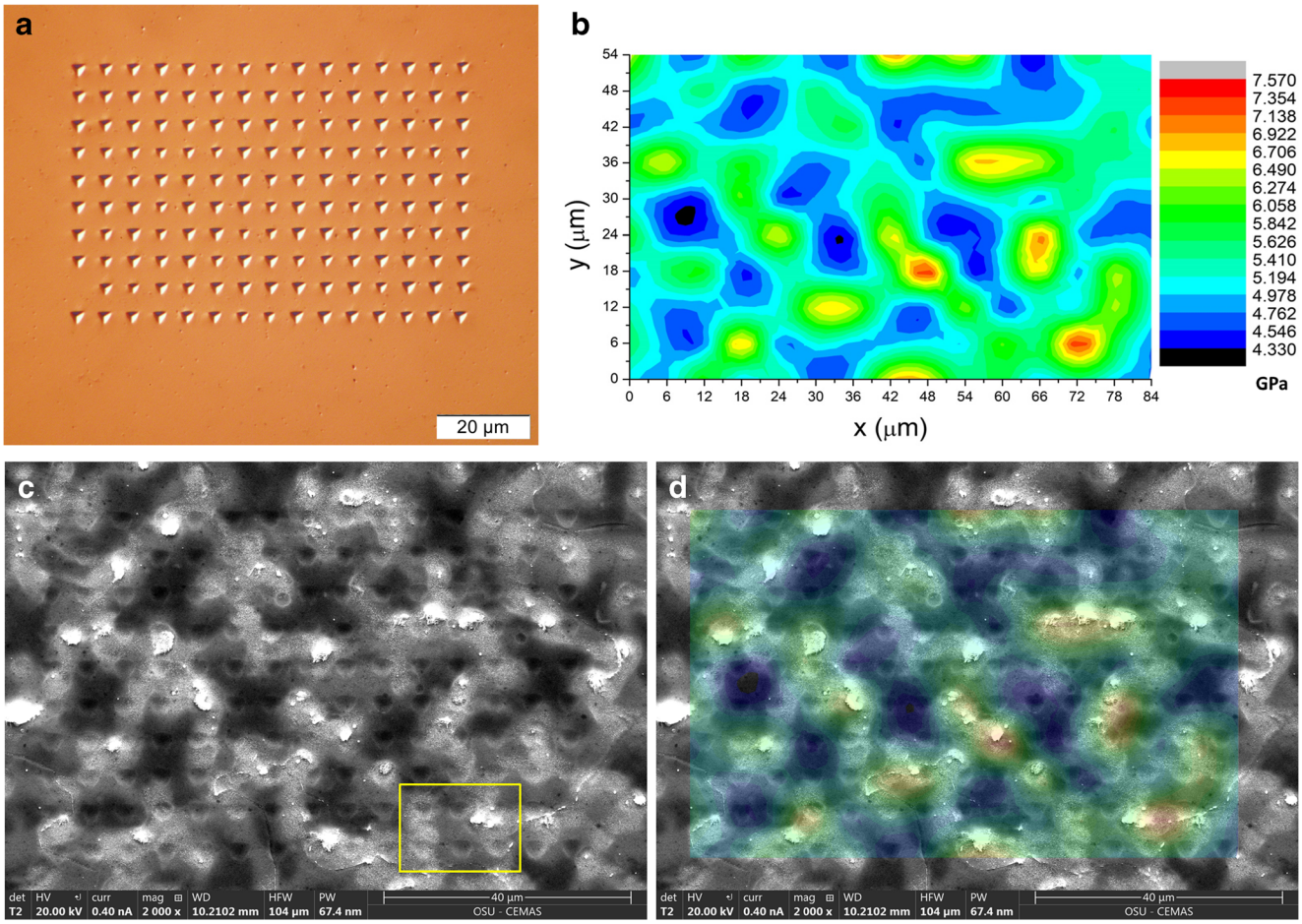

Fig. 8 **a**, **b** Nanohardness indent matrix and corresponding nanohardness map, **c** SEM photo of the indented area after etching, **d** overlapping of the hardness map with the microstructure

γ″ precipitates in Alloy 625 weld metal were observed in the interdendritic regions (richer in Mo, Ti, Nb) in aging conditions 1200 °F/100 h, 1300 °F/100 h, 1400 °F/10 h, and the nucleation of γ″ was observed at 1300 °F/10 h and

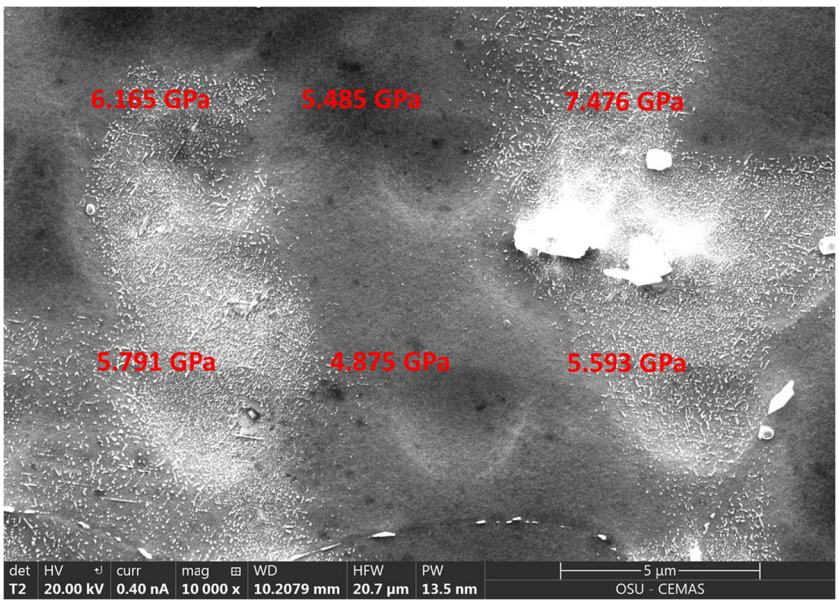

Fig. 9 Nanohardness values of several indentations in the yellow framed area in Fig. 8c

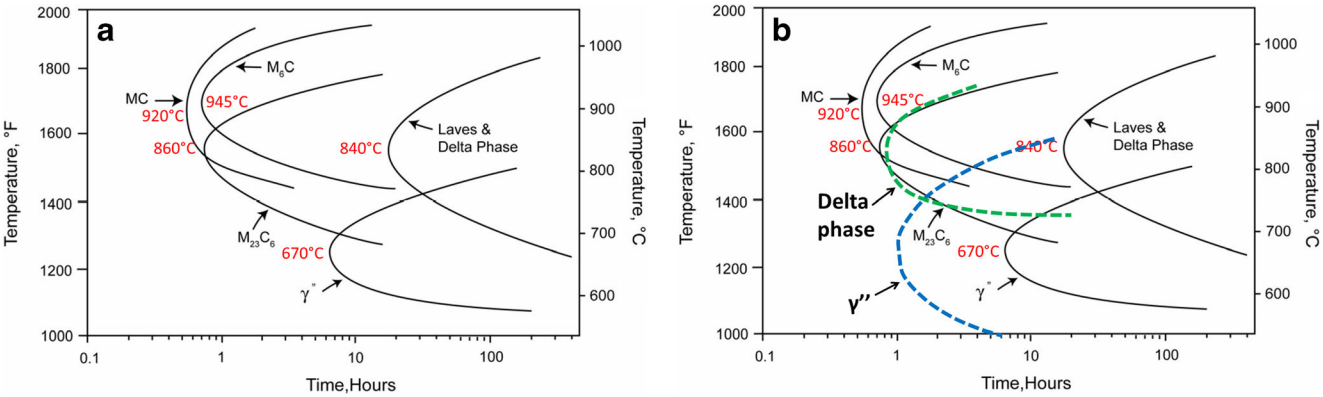

Fig. 10 **a** Time-temperature-precipitation diagram of wrought Alloy 625 [9], **b** estimated time-temperature-precipitation curve of γ″ and δ phases in the interdendritic regions of Alloy 625 weld overlay

1400 °F/1 h. Thus, the C-curve for the γ″ precipitation in weld metal is approximated by the dashed blue curve in Fig. 10b. δ phase precipitation in weld metal was observed to have started in aging conditions 1300 °F/100 h, 1400 °F/1 h, 1500 °F/1 h and 1600 °F/1 h. Thus, the C-curve for the δ phase is also shifted to lower temperatures and shorter times as shown by the dashed green curve.

The formation of γ″ involves nucleation and growth. The driving force for nucleation is undercooling below the equilibrium phase transformation temperature. Precipitate growth is controlled by diffusion. While cooling to a temperature below equilibrium transformation temperature provides a driving force for nucleation, lower temperatures reduce the rate of precipitate growth due to reduced diffusion. Thus, there is an optimum phase transformation rate at a critical undercooling temperature as shown in Fig. 11a. Therefore, the time-temperature-precipitation curve must be a long C-shape with a "nose" as shown in Fig. 11b, namely, the phase transformation time is shortest when the phase transformation rate is fastest [18].

As noted previously, the TTP diagram in Fig. 10 was developed using wrought Alloy 625 [9], which presumably contains more dislocations than the as-welded or as-solidified Alloy 625. The dislocations are the major nucleation sites for precipitates like γ″. Thus, the nucleation rate curve for Alloy 625 weld metal moves to even lower temperature and

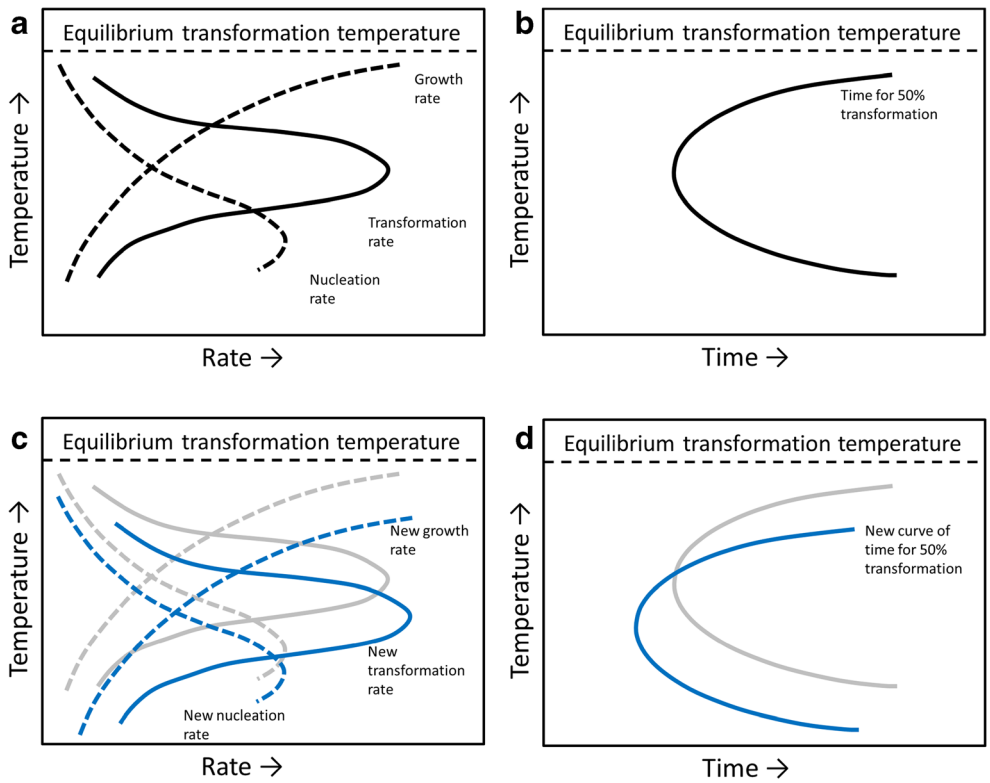

Fig. 11. **a** Variation of phase transformation rate with nucleation rate and nucleus growth rate, **b** sketch of a C-shaped TTP curve according to **a**, **c** the curve of phase transformation rate shifted in the interdendritic regions of Alloy 625 weld overlay; **d** TTP curve shift in the interdendritic regions according to **c**

results in additional undercooling for nucleation (Fig. 11c). EDX analysis shows that Alloy 625 weld metal has higher Nb, Ti, and Mo contents in the interdendritic regions than the normalized Alloy 625 composition. Thus, the interdendritic regions of Alloy 625 weld overlay require less diffusion for the precipitate growth, and the curve moves to lower temperatures (Fig. 11c). In general, the maximum phase transformation rate of γ″ moves to lower temperature. Probably, in the interdendritic regions of Alloy 625 weld overlay, the influence of high Nb, Ti, and Mo contents on diffusion is more significant than the influence of dislocation density, the maximum phase transformation rate also increased (Fig. 11c). Thus, the TTP C-curve moves down and to the left (Fig. 11d).

In the Alloy 625 overlay weld on the coke drum, the TTP C-curve of γ″ phase probably also moved down and to the left. This will shift the "nose" of the γ″ precipitation curve in Fig. 10 to the left and potentially widen the curve, thereby expanding the precipitation regime to lower temperatures—possibly to below 1000 °F. This explains why the peak temperatures experienced by the coke drum (885–930 °F) can result in γ″ precipitation and subsequent hardening during extended service exposure. Also, the cycling of the coke drum from room temperature to close to 1000 °F results in repeated expansion and contraction of the overlay. This mechanical "hot working" of the weld metal potentially increases the dislocation density in the overlay and contribute to a stronger precipitation reaction than that observed in the laboratory samples. This may explain why the service-exposed overlay is nearly 100 VHN higher than the laboratory samples.

5 Conclusions

A thermomechanically aged Alloy 625 overlay sampled from an industrial coke drum was characterized and compared to a variety of furnace-aged overlays to better understand the potential cause of cracking in a coke drum. The main conclusions from this investigation are the following.

1) Blocky particles (0.1–1 μm) were found in all Alloy 625 weld overlay samples. These are MC(N) particles of stoichiometry (Nb, Mo, Ti)(C, N) that form in the interdendritic regions by a eutectic reaction at the end of solidification.
2) γ″ and δ phase precipitation were observed in the interdendritic regions of various furnace-aged overlays due to relatively high Nb and Mo contents, approximately 6 and 12 wt%, respectively.
3) The dendrite core regions of the overlay were precipitate-free due to the low Nb content (~ 2 wt%) in these regions.
4) Precipitation of γ″ phase was initially found in aging conditions 1200 °F/100 h, 1300 °F/10 h, and 1400 °F/1 h in the interdendritic regions. A high density of γ″ precipitates was found in aging conditions 1300 °F/100 h and 1400 °F/10 h. Dissolution and coarsening of γ″ precipitates occurred when aging at 1500 and 1600 °F.
5) Precipitation of δ phase initially occurred in aging conditions 1400 °F/1 h, 1400 °F/10 h, and 1500 °F/1 h. Larger plate-like δ phase was found in 1500 °F/10 h, 1600 °F/1 h, and 1600 °F/10 h aging treatments.
6) Nanoindentation shows that the interdendritic regions with γ″ precipitates have much higher hardness than the dendrite core regions. The sample 1300 °F/100 h has the highest hardness due to an optimum size and distribution of γ″ precipitate. The samples aged in conditions 1500 °F/1 h, 1500 °F/10 h, 1600 °F/1 h, and 1600 °F/10 h have low hardness due to dissolution and coarsening of γ″ precipitates and formation of δ-phase which does not contribute to hardening.
7) The high hardness of the Alloy 625 weld overlay on the coke drum resulted from extensive γ″ precipitation. In the interdendritic regions, TTP curves for γ″ precipitation regions shifted to much lower temperatures allowing γ″ precipitation during service.

References

1. Shoemaker, L., Alloys 625 and 725: trends in properties and applications, in *Superalloys 718, 625, 706 and* Derivatives, TMS (The Minerals, Metals & Materials Society), 2005, pp. 409–418
2. Dai T, Lippold JC (2017) Tempering behavior of the fusion boundary region of an F22/625 weld overlay. Weld J 96:467–480
3. Dai T, Lippold JC (2018) The effect of postweld heat treatment on hydrogen-assisted cracking of F22/625 overlays. Weld J 97:75–90
4. Dai T, Lippold JC (2018) Tempering effect on the fusion boundary region of alloy 625 weld overlay on 8630 steel. Welding in the World 62(3):535–550
5. Dai T, Lippold JC (2018) The effect of postweld heat treatment on hydrogen-assisted cracking of 8630/alloy 625 overlay. Welding in the World 62(3):581–599
6. Lippold, J. C. and Wheeling, R. A.,2017 An investigation of alloy 625 weld overlay microstructure from a coke drum that experienced service cracking, unpublished
7. Brown EE, Muzyka DR (1987) Nickel-iron alloys. In: The Superalloys II. John Wiley, New York, pp 165–187
8. Sundararaman, M., Mukhopadhyay, P. and Banerjee, S.,1994 Some aspects of the heterogeneous precipitation of the metastable γ″ phase in alloy 625, in *Superalloys 718, 625, 706 and Various Derivatives*, E. A. Loria, Ed., Warrendale, PA, TMS, , pp. 405–418
9. Floreen, S., Fuchs, G. E. and Yang, W. J.,1994 The metallurgy of alloy 625, in *Superalloys 718, 625, 706 and Various Derivatives*, E. A. Loria, Ed., Warrendale, PA, TMS, pp. 13–38
10. Petrzak P, Kowalski K, Blicharski M (2016) Analysis of phase transformations in Inconel 625 alloy during annealing. Acta Phys Pol A 130(4):1041–1044
11. Shaikh MA, Ahmad M, Shoaib KA, Akhter JI, Iqbal M (2000) Precipitation hardening in Inconel* 625. Mater Sci Technol 16(2): 129–132

12. Suave LM, Cormier J, Villechaise P, Soula A, Hervier Z, Bertheau D, Laigo J (2014) Microstructural evolutions during thermal aging of Alloy 625: impact of temperature and forming process. Metall Mater Trans A 45(7):2963–2982
13. Malej S, Medved J, Batic BS, Tehovnik F, Godec M (2017) Microstructural evolution of Inconel 625 during thermal aging. Metalurgija 56(3–4):319–322
14. Mathew MD, Parameswaran P, Bhanu Sankara Rao K (2008) Microstructural changes in alloy 625 during high temperature creep. Mater Charact 59:508–513
15. Garzarotli F, Gerscha A, Francke FP (1969) Untersuchungen uber das Ausscheidungsverhalten und die mechanischen Eigenschaften der Legierung Inconel 625. Z Metallkunde 60:643–652
16. Silva CC, Miranda HC, Motta MF, Farias JP, Afonso CRM, Ramirez AJ (2013) New insight on the solidification path of an alloy 625 weld overlay. J Mater Res Technol 2(3):228–237
17. Inconel alloy 625 - special metals, [Online]. Available: http://www.specialmetals.com/assets/smc/documents/alloys/inconel/inconel-alloy-625.pdf
18. Bleck W (2007) Materials science of steel. RWTH Aachen University, Aachen, Germany, pp 270–271